DMD Fast Forward. Published on October 20, 2008 as doi:10.1124/dmd.108.023820
This article has not been copyedited and formatted. The final version may differ from this version.

Title Page

Discovering Plausible Mechanistic Details of Hepatic Drug Interactions

Tai Ning Lam and C. Anthony Hunt

The UCSF Program in Pharmaceutical Sciences and Pharmacogenomics, University of California, San Francisco, CA, USA 94143 (TNL, CAH)

Department of Bioengineering and Therapeutic Sciences, The BioSystems Group, The University of California, San Francisco, CA, USA 94143 (TNL, CAH)

Running Title Page

Running title: Mechanisms of Hepatic Drug Interactions

Corresponding author:

C. Anthony Hunt

Department of Bioengineering and Therapeutic Sciences

University of California, 513 Parnassus Ave., S-926

San Francisco, CA 94143-0912

P: 415-476-2455; F: 415-514-2008

<a.hunt@ucsf.edu>

Number of text pages: 23

Number of figures: 5

Number of tables: 5

Number of references: 19

Words in Abstract: 249

Words in Introduction: 701

Words in Discussion: 1,329

Abbreviations:

PK: pharmacokinetic; PRN: pseudo-random number; RISL: Recirculating In Silico Liver;

SD: standard deviation; SM: similarity measure.

DMD Fast Forward. Published on October 20, 2008 as DOI: 10.1124/dmd.108.023820
This article has not been copyedited and formatted. The final version may differ from this version.

Abstract

We sought a single set of mechanisms that could provide a quantitative explanation of three pairs of published time series data: perfusate concentration of digoxin and its metabolite in perfusates of isolated perfused rat livers 1) in the absence of any predose and with a predose of either 2) the uptake inhibitor rifampicin or 3) the efflux inhibitor quinidine. We used the synthetic modeling and simulation method because it provides a means of developing a scientific, experimental approach to unraveling and understanding some of the complexities of drug-drug interactions. We plugged together validated, quasi-autonomous software components to form abstract, but mechanistically realistic analogues of livers undergoing perfusion (Recirculating In Silico Livers: RISLs), into which we could add objects representing each of the above three drugs, alone or in combination. Each RISL was a hypothesis about plausible mechanisms responsible for the referent time series data. Simulations tested each hypothesis. We used Similarity Measures (SM) to compare results to the six sets of referent data. From many candidates, we identified a RISL having time-invariant mechanisms that achieved a weak Similarity Measure (SM-1), but failed to achieve a stronger Similarity Measure. Replacing four, time-invariant with time-variant mechanisms along with addition of new enzyme and transporter components, achieved the most stringent SM: simulated digoxin and metabolite perfusate levels were experimentally indistinguishable from the referent data, for all three treatments. The mechanisms simulated unanticipated loss of hepatic viability during the original wet-lab experiments: erosion of hepatic accessibility and of enzyme and transporter activities.

DMD Fast Forward. Published on October 20, 2008 as DOI: 10.1124/dmd.108.023820
This article has not been copyedited and formatted. The final version may differ from this version.

Introduction

Given the variety of transporters and enzymes that can be involved, how can we enhance substantially our ability to confidently anticipate the consequences of hepatic drug-drug interactions in advance of costly wet-lab experiments? To do so, we need improved knowledge of multi-level spatiotemporal mechanistic details. We need new classes of models with capabilities beyond those of the current pharmacokinetic (PK) and pharmacodynamic variety, plus methods to more realistically represent critical spatiotemporal details, all within single model systems. Finally, we must be able to explore realistic, concurrent, interaction consequences of two or more drugs when given key physicochemical properties, which is infeasible using current PK models. An essential first step in realizing those needs is to demonstrate a fine-grained, computational analogue in which measures of simulated interactions of two drugs are experimentally indistinguishable from those of referent wet-lab experiments. When the analogue's assembled components map realistically to hepatic components, and the measured consequences of in silico and wet-lab mechanisms are indistinguishable, we can posit that the responsible mechanisms of both systems are similar, as diagrammed in Fig. 1. Achieving these important goals has been an objective of this project.

The referent wet-lab experiments for this project used an ex vivo, perfused rat liver protocol to measure interactions between digoxin, rifampicin, and quinidine. The mechanisms are relatively well understood (Lau, et al. 2004). Digoxin, a P-glycoprotein substrate (de Lannoy and Silverman, 1992), is transported basally in hepatocytes by Oatp2 (slc21a5) (Noe et al., 1997). Because rifampicin is an Oatp2 inhibitor and quinidine is a P-glycoprotein inhibitor, the disposition properties of digoxin are altered when it is co-administered with either.

The synthetic method of modeling and simulation (Hunt et al., 2006), (Yan et al., 2008a), (Yan et al., 2008b), also called executable biology (Fisher and Henzinger, 2007), (Hunt et al., 2008), offers advantages over traditional methods for exploring and testing hypotheses about mechanisms. Traditional PK models formulate hypotheses about data, whereas the assembled components of a synthetic model are

DMD Fast Forward. Published on October 20, 2008 as DOI: 10.1124/dmd.108.023820
This article has not been copyedited and formatted. The final version may differ from this version.

a testable mechanistic hypothesis about spatiotemporal details underlying that time course data. Execution tests that hypothesis. Measures of analogue attributes can overlap corresponding measures of referent attributes. Measures of attribute similarity provide a quantitative means of accepting or rejecting the hypothesis.

We used the synthetic method to construct and verify liver analogues suitable for simulating recirculating liver perfusion experiments. They were similar to, but simpler than, the one used in (Yan et al., 2008a). The result was the Recirculating In Silico Liver (RISL) diagrammed in Fig. 2. Objects representing Oatp2s and P-glycoproteins were included within separate (membrane) spaces. Cell interiors and perfusate contained objects responsible for nonspecific drug binding. Different objects represented drug-metabolizing enzymes. Spaces were designated to represent bile and perfusate. Three different mobile objects carried information identifying each as representing digoxin, rifampicin, or quinidine (Lau, et al. 2004). RISL components used that information to distinguish between them.

We started with a simple, time-invariant RISL having five spaces along with components representing digoxin, two inhibitors, CYP3A enzymes, Oatp2s, and P-gps. RISL disposition profiles of rifampicin and quinidine were similar to the reported liver profusion profiles. Disposition and metabolite formation profiles for digoxin, administered alone, were also acceptable matches to liver perfusion profiles, using a quantitative similarity measure. However, corresponding profiles following a pre-dose of rifampicin or quinidine were completely dissimilar to referent values: because implemented mechanisms were too simple, that initial RISL failed to simulate observed drug interactions. Adjusting that RISL's spatial, component, and interaction details, failed to uncover plausible explanations. A protocol was followed for adding additional mechanistic complexity. It used three, increasingly stringent measures of similarity. Postulating time-dependent changes in specific details, including simulating hepatic injury, erosion in the quality of regional hepatic perfusion and increasing loss of hepatic viability dramatically improved the quality of match. It took the combination of four different time-dependent changes for the RISL profiles to achieve the most stringent similarity measure, yet changes in hepatic physiology were not evident during wet-lab experiments.

Because wet-lab model systems are artificial, measures are taken to minimize change, yet some may go undetected and can influence observables. The methods used uncovered such changes thereby providing deeper insight into plausible drug-drug interaction mechanisms, even though the nature of some was unexpected.

Methods

To distinguish clearly in silico components and processes from corresponding hepatic components and processes, we use SMALL CAPS when referring to the former. In contrast to inductive models, which often focus on prediction, the RISL and its method have been designed for discovering and testing plausible, detailed mechanistic explanations of hepatic drug disposition and interaction data. A specific RISL instantiates a hypothesis (Fisher and Henzinger, 2007), (Hunt et al., 2008). Execution and comparison of results to referent counterparts tests the hypothesis.

Objective and Approach. Our objective was to discover a single parameterized set of multi-level hepatic mechanisms that would provide one plausible explanation for the three pairs of the time series data in Fig. 3, while achieving a stringent measure of similarity as described below. One pair of time series data describes the PK and metabolism of digoxin administered alone. The other two are measures of the PK and metabolism of digoxin when the livers were predosed ten minutes earlier with rifampicin or quinidine. We were not seeking a traditional, differential equation explanation of time course data. Rather, we sought an actual, working mechanism—*an analogue*—comprised of quasi-autonomous processes and parts, which when measured during execution would give time course data similar to wet-lab data in Fig. 3. Our technical approach used the synthetic modeling and simulation method (Hunt et al., 2006): we plugged together validated, quasi-autonomous software components to form an abstract, but mechanistically realistic analogue of a liver undergoing perfusion into which we could add, alone or in combination, objects representing the three different drugs: digoxin, rifampicin, and quinidine. Our experimental approach followed an iterative sequence: RISL synthesis, testing and evaluation, validation or falsification, assessment, cogitation, and system revision.

Hunt et al. (Hunt et al., 2006) and Yan et al. (Yan et al. 2008a), (Yan et al., 2008b) describe an In Silico Liver comprised of similarly constructed LOBULES. Because perfusate was recycled in the wet-lab experiments, the data did not require that level of detail, so we designed, validated and used a simpler in silico liver. The rationale for doing so is expanded upon in Supplemental Material—hereafter Supplement. During RISL design, our focus was on simplicity. Parsimony is important. Traditional PK modeling strives to avoid overparameterization. By analogy, synthetic modeling strives to avoid overmechanization. We decided to abstract away the complex lobular architecture and interconnected sinusoidal networks and use only five separate spaces in the initial RISL. One (S1) would represent perfusate and extracellular fluid. A second (S2) would represent the barrier (not limited to just cell membranes) between perfusate and cell interiors that would be represented by a third space (S3). A fourth (S4) was needed to represent the barrier between bile and cell interiors. The fifth (S5) represented bile. Although there was no referent bile data, S5 was needed as the location for COMPOUND elimination. The temporal resolution of the data in Fig. 1 was insufficient to distinguish and validate separate representations of a layer of endothelial cells, the space of Disse, and hepatocytes. Consequently, we conflated their representation. The resulting five spaces can be viewed as a tube comprised of a layer of CELLS (S2, S3, and S4, representing primarily hepatocytes), flanked by PERFUSATE and rapidly equilibrating EXTRACELLULAR FLUID (S1) on the "basal" side and BILE (S5) on the "apical" side. Together the five spaces function as a simplified analogue of a hepatic lobule, or a portion thereof. As in (Hunt et al., 2006), we pooled or averaged results from *n* Monte Carlo LOBULE variants to represent an entire RISL. Drawing on results of early simulations, we decided that $n \geq 6$ were adequate for the objective (experimental results supporting that choice are provided in Supplement). The referent wet-lab experiments used $n = 6$. As in the above-cited In Silico Liver, we specified three categories of components: spaces, active objects and passive objects. They are listed in Table 1. Primary parameter values are listed in Table 2. Additional information is provided in Supplement.

DMD Fast Forward. Published on October 20, 2008 as DOI: 10.1124/dmd.108.023820
This article has not been copyedited and formatted. The final version may differ from this version.

Model Structure and Components. S1–S5, sketched in Fig. 2, have been implemented as two-dimensional, toroidal grids having identical granularities. Grid granularity (grid dimensions) is parameter controlled. Simulation run time is proportional to grid size, and measurement variance increases with decreasing grid size. The exploratory nature of parameter tuning and iteratively revising analogues necessitates running many simulations. Balancing these considerations, we settled on a 50x50 grid size for all experiments.

At each grid location, we placed an object that functions as a container for other objects. We call it an ELEMENT (of that space). Each of the 2,500 S3 ELEMENTS mapped to a portion of a lobule's intracellular content. ELEMENTS in S2 and S4 mapped primarily to portions of cell membranes, including hepatocyte apical and basal membranes, along with some of the adjacent material. All TRANSPORTERS were placed randomly and uniformly within these two spaces. S2 also mapped to features of the sinusoidal endothelial layer and the adjacent space of Disse. However, such detail was below RISL resolution. Each S5 ELEMENT mapped to a portion of bile, and an ELEMENT of S1 mapped to portion of perfusate plus the rapidly equilibrating extracellular spaces (hereafter referred to as PERFUSATE). An ELEMENT can be identified and labeled with relevant chemical properties. For example, each element of S1 can be assigned whatever referent properties are required for the experiments planned, such as pH, ionic strength, etc. These properties can be made different for S5 (BILE).

ELEMENTS can contain mobile and stationary objects. We included only objects that proved necessary to achieve our objective. Unlike with traditional physiologically based PK models, new components can be added without interfering with the function of those already present. A COMPOUND (also called DRUG) was a mobile object that mapped to a small fraction of the drug added to perfusate at t = 0, or, in the case of METABOLITE, generated within hepatocytes. As in previous reports (Hunt et al., 2006), (Garmire et al., 2007), (Yan et al., 2008a), (Yan et al., 2008b), one COMPOUND mapped to a large but unspecified number of actual referent molecules. A RISL used four types: DIGOXIN, METABOLITE (of DIGOXIN), RIFAMPICIN, and QUINIDINE. Their RISL properties are listed in Table 3 along with referent's properties. To enable each RISL stationary object to distinguish different types of mobile objects, each

COMPOUND carries identification; it could include values representing several of the referent compound's properties. RISL stationary objects were given logic (diagrammed in Supplement Fig. S2) that enabled them to use a COMPOUND'S properties to control how they interacted with COMPOUNDS. For examples, see (Yan, et al., 2008b), (Sheikh-Bahaei and Hunt, 2006). Parameter values were tuned separately for each COMPOUND. Each COMPOUND, selected randomly, has one opportunity to relocate during each simulation cycle. Six simulation cycles mapped to one minute of wet-lab time. A COMPOUND relocation event was subject to the COMPOUND'S local environment. That process was a variation on those used previously and cited above. A detailed description is provided in Supplement. An abridged description follows.

TRANSPORTERS, BINDERS, and CYP. An RISL uses three classes of active, stationary objects. One maps to transporters. The second, CYP, maps to the enzymes responsible for digoxin metabolism, primarily CYP3A. The third class is BINDERS; they map to anything within a lobule or perfusate that might bind or sequester compounds. The logic used by each is diagrammed in Supplement Fig. S2 along with additional validation evidence. We implemented initially two types transporters: PGP and OAT. PGP maps to P-glycoprotein and any other transporters responsible for efflux of digoxin from hepatocytes to bile. OAT maps to Oatp2 and any other transporters that are responsible for the active cellular uptake of digoxin. However, the details of PGP and OAT operations were below the level of resolution and so do not map to biochemical counterparts.

CYP binding sites within a CYP are identical and independent. As with PGP and OAT, details of CYP operations are below the level of resolution and so do not map to biochemical counterparts. CYP parameter values are listed in Tables 2, 4 and 5. At the start of a simulation, all CYPS were assigned randomly and uniformly to elements within S3. Each simulation cycle, each CYP steps through its assigned logic to determine what action to take. It examines its adjacent neighborhood. Neighborhood size is controlled by *sitesN*. The probability that a CYP-DRUG binding event will occur for any DRUG within a CYP'S neighborhood is governed by *assocProb* (Table 4), the value of which maps to affinity. A CYP can bind any

DMD Fast Forward. Published on October 20, 2008 as DOI: 10.1124/dmd.108.023820
This article has not been copyedited and formatted. The final version may differ from this version.

COMPOUND that has a non-zero *assocProb*, whether it is a substrate or not. However, only substrates are METABOLIZED. The frequency at which METABOLISM occurs is controlled by the tunable METABOLIC parameter *efficiencyProb*. After that, each CYP examines each bound COMPOUND; each is given an opportunity to be RELEASED within that same cycle. That process is governed by *releaseProb* (Table 4). When the COMPOUND is a substrate, the released object may be a METABOLITE.

Each PGP and OAT functions similar to CYP; there are differences. Table 4 shows that *isaSubstrate*, *assocProb*, and *releaseProb* are tuned to different values for PGP, OAT, and, CYP as well as for the different COMPOUNDS. PGPS are assigned randomly and uniformly to S4. They look for COMPOUNDS in S3. When one is found and the value of *assocProb* is non-zero, it is given an opportunity to bind. However, only substrates are TRANSPORTED to S5; the COMPOUND'S property list is checked to determine if *isaSubstrate* is true for PGP. If so, it qualifies as a substrate and has an opportunity to be TRANSPORTED to S5. Analogously, OATS were assigned randomly and uniformly to S2. They look for COMPOUNDS in both S1 and S3. When one is found and *assocProb* $\neq 0$, it is given an opportunity to bind. If *isaSubstrate* is true for OAT, it qualifies that COMPOUND as a substrate and it is given an opportunity to be TRANSPORTED. Frequency of release into the space of destination is controlled by *efficiencyProb*. When PGP and OAT find and bind a non-substrate, such as an inhibitor, it is always released in a subsequent simulation cycle to the space from which it was bound. Additional detail is provided in Supplement.

A BINDER is an object that functions logically similar to CYP, except that it does not metabolize. It simply binds and later releases the COMPOUND. BINDERS can be added to any ELEMENT, but in these RISLs, they have been confined to S1 and S3. A BINDER'S logic is diagrammed in Supplement, Fig. S2. Briefly, a BINDER searches its assigned neighborhood for a COMPOUND. For each one found, its property list is scanned. If the COMPOUND qualifies for binding, it is given an opportunity to bind. If bound, it will be released in a later simulation cycle. Binding and release events for each site are controlled by the BINDER and COMPOUND-specific values of *assocProb* and *releaseProb* listed in Table 4.

DMD Fast Forward. Published on October 20, 2008 as DOI: 10.1124/dmd.108.023820
This article has not been copyedited and formatted. The final version may differ from this version.

Tunable Parameter Values and Movements of COMPOUNDS. Most events, such as a COMPOUND binding to CYP, are probabilistic and have values in the 0–1 range. When an event option arises, a pseudo-random number (PRN) is drawn from a range such as 0–1. Its value is compared to that of the parameter to decide what action to take. For example, if the PRN is less than the value assigned to *assocProb*, the event occurs. Else, it does not.

The percolation of compounds through lobular spaces during perfusion is simulated by individual movements of unbound COMPOUNDS. The logic governing COMPOUND movement is adapted from the validated logic used previously and is diagrammed in Supplement Fig. S2, where additional details are also provided. Briefly, each cycle, unbound COMPOUNDS are given an opportunity to move. Next, TRANSPORTERS, CYP, and BINDERS are given opportunities to bind and then release COMPOUNDS. The order in which COMPOUNDS are updated is randomized each cycle independent of the space in which they are located. A COMPOUND first has an opportunity to relocate laterally or stay in its current ELEMENT. The current and eight adjacent ELEMENTS are each assigned one of nine integer values 1–9. A PRN is drawn randomly from [1–9]; the COMPOUND moves to the ELEMENT assigned the same integer value. Following that, the COMPOUND has an opportunity to move into an adjacent space.

To transit across a barrier, a COMPOUND must be sufficiently close to the interface. To represent that, we use the probability parameter, *closetoInterface*. The barriers to which S2 and S4 map are represented as being very thin (less capacity) relative to S1, S3, and S5. For simplicity, given the fact that a simulation cycle maps to 10 seconds, we specified *closetoInterface* = 1 for all COMPOUNDS in S2 and S4. For a COMPOUND in S1, S3, and S5, if a PRN < *closetoInterface*, the COMPOUND is given an opportunity to transition; else, it stays put. The probability that a transition will actually occur, given the chance, is specified by another parameter *transitProb*. As done with *closetoInterface*, we estimated an initial value using the COMPOUND's properties (see Supplement) for each transition; when needed, that estimate was tuned. The values listed in Table 3 proved adequate for achieving targeted Similarity Measures. The sequence in which each COMPOUND'S transit decision was made followed the same pattern for each space; it is discussed in Supplement.

DMD Fast Forward. Published on October 20, 2008 as DOI: 10.1124/dmd.108.023820
This article has not been copyedited and formatted. The final version may differ from this version.

Simulated Perfusate Flow. Perfusion experiments started with the dose being added to the reservoir. Because the flow rate was 40 ml/min, a second or two later, drug-free perfusate entered the reservoir from the liver as drug-containing perfusate was entering the liver. There was a short interval in which drug rapidly distributed into easily accessible extracellular spaces. A few seconds later those spaces were mostly occupied by drug. Thereafter, perfusate compound levels continued declining, but within a 10-second simulation cycle, the difference between entering and exiting drug levels rapidly shrank to within the range of wet-lab analytical sensitivity. Following early exploratory simulations, we estimated that during that initial, rapid distribution phase, about 13% of the dose had been retained within hepatic spaces (was *internal*). At that stage, drug that had not already transitioned into cells was essentially in one of three states: 1) *external* (to the liver), 2) within extracellular hepatic spaces but not likely to transition across cell membranes within the next 10 seconds (*internal*), and 3) within the liver and sufficiently close to cell membranes so that transition within the next 10-second was possible (*transitional*).

We considered several options to simulate the preceding scenario. One option would be to simulate flow within the space (e.g., S1) representing perfusate, analogous to how it was done in (Hunt et al., 2006). S1 could be made circular and much larger than the HEPATIC spaces. COMPOUNDS could move around the circular space simulating flow. Another option is discussed in Supplement. To keep the RISL relatively simple, all that was needed was to distinguish the portion of the PERFUSATE that was external to the LIVER at each sampling time. The COMPOUNDS that were randomly assigned to S1 were simply specified as being in one of three states, *external*, *internal*, and *transitional*; and every compound in S1 had an opportunity to change its state each cycle. Changing state simulated both perfusate flow and rapid equilibration between perfusate and hepatic spaces. The parameter *internalProb* specified the probability that a COMPOUND in S1 would be designated internal within a simulation cycle. Changing *internalProb* simulated a change in perfusate flow rate. The parameter *closeToInterface* specified the probability that a COMPOUND in S1 would be *transitional* (available to transition to S2). The balance of COMPOUNDS in S1 was *external*. For most of the RISL simulation results discussed below, *internalProb* = 0.13. BINDERS

DMD Fast Forward. Published on October 20, 2008 as DOI: 10.1124/dmd.108.023820
This article has not been copyedited and formatted. The final version may differ from this version.

were randomly assigned to S1 and so a small fraction of COMPOUNDS was bound and thus neither available to partition into S2 nor be taken up by an OAT.

When an experiment called for pre-doses of either RIFAMPICIN or QUINIDINE interacting with DIGOXIN, the inhibitor was added to S1 first. The simulation was then run for an additional 60 simulation cycles (10 MINUTES), at which time the simulation was stopped, DIGOXIN was added, and the simulation was re-started.

Targeted Attributes are Objectives to be Achieved. An early protocol task was to specify a target set of phenotypic attributes, and have in mind additional attributes that could be sequentially added to the target list (Hunt et al., 2006), (Tang et al., 2007). The goal was to find RISL parameterizations such that measures of simulation attributes, such as METABOLITE levels in PERFUSATE, would be similar to targeted wet-lab attributes in some specified way. Our initial set of four targeted attributes was simple (thus less demanding) and did not include the entire time-series profiles. They were 1) the fraction of the digoxin dose remaining in perfusate after 60 minutes, 2) the corresponding perfusate level of metabolite, 3) the increase in 60-minute metabolite levels in the presence of quinidine (assuming significant inhibition of P-glycoprotein), and 4) the decrease in 60-minute metabolite levels in the presence of rifampicin (assuming significant inhibition of Oatp2). A parameterized RISL that achieved those objectives was valid for the targeted attributes. Next, our goal was to expand the attribute list by adding all time-series observations. The final goal was to obtain one RISL, which when dosed with combinations of the three simulated drugs, would generate behaviors that were experimentally indistinguishable from the time series data in Fig. 3. At first glance, the preceding four criteria seem lax. That proved not to be the case. Explanations are provided in the next section.

Achieving Similarity Measures. Specifying a similarity measure (SM) is arbitrary. Three were used. They ranged from least stringent (SM-1) to most stringent (SM-3). We started with SM-1. Once that was achieved, we switched to SM-2, followed by SM-3. Once a SM was achieved, we could state that the

DMD Fast Forward. Published on October 20, 2008 as DOI: 10.1124/dmd.108.023820
This article has not been copyedited and formatted. The final version may differ from this version.

RISL had been validated against the available data using that SM criterion. Of course, switching to a more stringent SM may have falsified that RISL.

The targeted attributes coupled all three pairs of time course data. That required one RISL be used to simulate outcomes of all three treatments. If a parameter change was made to improve, for example, the match to metabolite data following treatment with rifampicin, all of the other five trajectories were also altered. The actual mechanisms responsible for the data in Fig. 3 were complex, multilevel, and fine-grained (more so than the RISL). Because the RISL is abstract and course-grained, it was not clear what level of mechanistic detail would be needed to achieve SM-3.

The wet-lab experiments achieved average mass balances of 89 to 91%. Consequently, a requirement of all SMs was that the simulation dose be within 10% of the stated, administered dose (see Supplement for additional details). Consequently, DOSE and other parameters were tuned within narrow ranges to achieve targets. The reported coefficient of variation for wet-lab values averaged 6.8% for perfusate digoxin values and 13.2% for metabolite values. To specify a target range, we assumed that repeated wet-lab measures would be normally distributed. We wanted RISL values to be well within ± 2 SD, based on the reported variances stated above. The target range for DIGOXIN was to be within 10% of mean, referent wet-lab values; and within 25% for METABOLITE. SM-1 focused just on the wet-lab values at 60 MINUTES: qualitatively, all three pairs of simulated measures needed to exhibit all four target attributes listed above; and quantitatively, mean RISL PERFUSATE DIGOXIN values at 60-minute needed to fall within 10% of the corresponding mean wet-lab values and within 25% for the METABOLITE values.

SM-2 required that SM-1 be met, and at least 46 of 51 (about 90%) of RISL values (DIGOXIN plus METABOLITE) must be within the target range. This criterion could be achieved by obtaining a good match to all three sets of digoxin time course values and only one set of metabolite time course values. SM-3 required that SM-2 be met, and that for each of the six time course profiles, no more than one measurement would be outside the above target ranges. A simulation result that achieved SM-3 was deemed experimentally indistinguishable: it would have been statistically indistinguishable from the results of a repeat experiment adhering to the original wet-lab protocol under identical conditions.

DMD Fast Forward. Published on October 20, 2008 as DOI: 10.1124/dmd.108.023820
This article has not been copyedited and formatted. The final version may differ from this version.

Tuning and Refinement. We started with 50 of each type of stationary object. We divided BINDERS between S1 and S3 based of a ballpark estimate of the relative amount of protein in hepatic cells and in perfusate: we initially placed 95% in S3 and 5% in S1. Most parameters having a 0–1 range were set initially to 0.5. The inhibitors were initially given higher affinities (0.9 or 1.0) and low release probabilities (0.1 or 0.01). Thereafter, a standard parameter-tuning protocol was followed iteratively: 1) simulate, 2) validate or falsify: if the specified SM was not met, then the RISL was falsified. 3) When falsified, diagnose (e.g., an observed mismatch between in silico and wet-lab results may have been caused by specific defects in RISL mechanisms), 4) hypothesis (e.g., the discrepancy will be reduced by specific RISL parameter adjustments or a change in the analogue's structure), 5) testing (repeat steps 1 and 2: contrast new simulation results with those from the predecessor RISL and with wet-lab results), 6) return to step three, or when the SM is achieved and the RISL validates, stop.

Time-dependent Parameter Changes. Despite intensive exploration of the RISL parameter space, we failed to find a time-invariant parameter vector that would enable achieving SM-2. To do so, the only obvious option was to increase RISL complexity, one alteration at a time, until first SM-2 and later SM-3 could be achieved. That process is described in Results; it too followed the tuning and refinement protocol. One new component was needed: it mapped to efflux transporters for the digoxin metabolite, and was called MT. It resided in S2 and functioned identical to PGP; it moved only METABOLITES from S3 to S1. In addition, we found it necessary to enable four parameter values to change unidirectionally with time. Those changes required adding additional parameters to manage the time-dependent changes. Selection of parameters to become time-dependent was done iteratively, one at a time. Each change was preceded by a hypothesis: increasing (or decreasing this parameter over 60 MINUTES will measurably improve the degree of similarity between simulated attributes and the wet-lab counterparts (sufficiently so that a statistical test was not needed to confirm that an apparent improvement was real). The simulation results provided a test of that hypothesis.

Software. The RISL was built from the Swarm platform and libraries (http://swarm.org). We coded in Java Swarm. Most experiments used a single processor and ran under Microsoft Windows XP with Java SDK and J2RE installed. Source code was compiled with Java 2 Software Development Kit SE v1.4.2_13, and executed with Java 2 Runtime Environment v1.4.2_13, (www.java.com). Output data files were processed, graphed and analyzed with Microsoft Excel and S-plus (Insightful). We repeated simulations six or more times. Results are reported as arithmetic mean values, unless otherwise noted. We assumed that the central limit theorem held for all observations. All pseudo-random number generation used Swarm's Mersenne Twister algorithm; the initial seed was extracted from the machine's clock. All PRNs were drawn from uniform distributions. Random integers were drawn from a uniform distribution between [min, max], inclusive. Random floating-point numbers were always drawn from a uniform [0.0, 1.0)—including 0.0, excluding 1.0.

Results

Overview. Our plan was to proceed through three stages marked by achieving increasingly stringent SMs. The stage one objective was to discover a RISL composition (numbers of RISL components and their location) and a parameterization that would produce simulated results at 60 MINUTES that met SM-1. The expectation was that once it was achieved, RISL alterations and reparameterizations could be found that would move RISL behaviors closer to SM-2 and, later, SM-3. Prior to achieving a SM, the RISL was a hypothesis: average results of at least six Monte Carlo experiments will achieve the stated similarity criterion. Simulation results stood as a test of that hypothesis, and a validated mechanism provided new knowledge.

Because a RISL is abstract and relativistic, we do not require one-to-one correspondence of components or observables between it and the wet-lab system. The goal was that relative, measured RISL behaviors be similar to those of the referent with the expectation that the two mechanisms will have features in common, as illustrated in Fig. 1. To facilitate that process, the original perfusate and metabolite data were transformed to values of fraction of administered dose.

DMD Fast Forward. Published on October 20, 2008 as DOI: 10.1124/dmd.108.023820
This article has not been copyedited and formatted. The final version may differ from this version.

Only one RISL was used. The only difference between experiments was the nature of the inhibitor PREDOSE. Changing a parameter value to improve the match to one time course always changed the other five. That coupling shrank the region of parameter space that would enable meeting a SM. It also dramatically limited the shapes of the simulated time course profiles. For many RISLs, there was no region of its parameter space that would enable meeting SM-2 or SM-3.

The steps taken to achieve SM-3 are detailed below. The results are graphed in Fig. 3.

Separate Disposition of RIFAMPICIN and QUINIDINE Implemented. To mimic the wet-lab protocol for two of the three treatments, RIFAMPICIN and QUINIDINE were administered separately prior to DIGOXIN dosing. We then tuned RISL's drug-specific parameter values until we obtained simulated PK time course data for each that was similar to reported data. Time course data for RIFAMPICIN and QUINIDINE administered alone are provided in Supplement Fig. S5. Those profiles were strikingly similar to corresponding referent quinidine and rifampicin profiles (Lau et al., 2004) without having either undergo METABOLISM. That similarity indicates that RIFAMPICIN and QUINIDINE metabolism, if measurable, was very modest. Consequently, to preserve simplicity, we elected not to complicate the analogue further by implementing a small degree of clearance for either RIFAMPICIN or QUINIDINE.

A simpler way to represent interaction with DIGOXIN would have been to deactivate all OAT to simulate complete inhibition by RIFAMPICIN, and deactivate all PGP to simulate inhibition by QUINIDINE. However, by so doing, we would have abstracted away (thereby making assumptions about) potentially important drug interaction details. Having the means to explore drug-drug interactions in some detail was a driving motivation for engineering the RISL as we did.

A Simple Hypothesis Fails. Supplement Fig. S7 shows results that satisfy the SM-1 criterion, but failed to satisfy SM-2; that RISL's composition and time-invariant parameter values are given in Supplement Table S1. We refer to that RISL as the simple, linear hypothesis. It included OAT, PGP, and CYP. We explored a wide variety of time-invariant parameter settings and a range of relative ratios and amounts of OAT, PGP, and CYP. No parameter vector was found that was able to provide adequate

similarity at early times (and thus possibly achieve SM-2) while still meeting SM-1. We concluded that a somewhat more complicated set of mechanisms would be needed. Note that the RISL is capable of generating a wide variety of PK profiles (that could be fit using one, two, or more exponentials). The failure of the simple RISL to achieve SM-2 is because its mechanisms were too few and/or too course-grained. We next considered a variety of mechanistic changes, extensions, and additions separately with the goal of improving the degree of match at early times, while still achieving SM-1. None worked. Nevertheless, we describe two that were thoroughly explored to provide background and a context for the changes that followed.

Two Mechanistic Changes to Improve RISL's Behaviors. First, we considered that metabolite might compete with digoxin for uptake transporters, slowing digoxin uptake as metabolites accumulate in the perfusate. We implemented the mechanism, specifying a bidirectional OAT, with METABOLITE being an OAT substrate. We explored the expanded parameter space (results not shown). In the absence of an INHIBITOR PREDOSE (the control), early DIGOXIN levels did move closer to referent values. However, in the case of EFFLUX inhibitor (QUINIDINE) PREDOSE, more METABOLITE formed (compared to no pretreatment), causing more inhibition of DIGOXIN uptake, which was inconsistent with the data.

Might a different transporter facilitate rapid metabolite efflux from cells to perfusate causing early, rapid accumulation of metabolite in perfusate? We created a METABOLITE TRANSPORTER and called it MT, and added it to S2. We explored a variety of parameterizations and found several that caused much higher, early PERFUSATE METABOLITE levels. Adding this new mechanism had moved us much closer to satisfying SM-2, but not close enough.

In the above scenarios, RISL mechanisms were unchanged during execution. We speculated that in the referent experiments that might not have been the case: mechanisms and component behaviors may have changed during the course of the experiments. We selected the simple RISL from above, which included MT, that exhibited the properties closest to SM-2 and asked, what time-variant mechanistic changes might lead to achieving SM-2 (and even SM-3)? In the absence of a PREDOSE, more DIGOXIN

accumulation in S3 would be needed and that would need to be coupled with more METABOLITE entering PERFUSATE. We began exploring how to achieve those two attributes.

Implementing Mechanistic Deterioration Improved Similarity. We pondered: ex situ, the liver might be deteriorating during the perfusion experiment, even though there was no reported evidence indicating so (Lau et al., 2004). Ischemic deterioration alone could cause a variety of influential changes, including changes in flow paths, cellular volume, accessible sinusoidal surface area, homeostatic metabolism, and microarchitecture (Straatsburg and Frederiks, 1997), (Bailey and Reinke, 2000). Such change could go unobserved during the course of an experiment, and yet alter enzymatic and transport functions. Plausible, yet unobserved, changes include transporter visibility to digoxin being reduced because fenestra frequency and cross-connections between sinusoids could have been reduced. Digoxin metabolism could decreases because some CYP450 (and/or cofactor) functions became defunct.

We used the inductive method to first identify and then explore several mechanistic changes in line with the above ideas. The following four were aggregated together and implemented. Results following RISL implementation, refinement, and parameter tuning met SM-2 and later enabled achieving SM-3. Results that achieved SM-2 are presented in Supplement Fig. S8. Alterations such as changes in digoxin-accessible sinusoidal surface area, reduced flow in some lobules, decreased fenestrae size or relative density, and/or altered sinusoid microarchitecture were conflated and represented together as a decrease in the effective surface area accessible to COMPOUNDS. This change was implemented by decreasing the value of *closeToInterface* and thus the fraction of dose in S1 that was in the *transitional* state during a simulation. It was reduced using a rapidly decreasing scaling factor. The scaling method is detailed in Supplement. We found it most effective (in achieving closer matches to earlier digoxin perfusate levels) to have most of the decline occur within the first five MINUTES. Behavior of the version used to achieve SM-3 is graphed in Fig. 4A.

Decreases in effective, accessible membrane surface area and cell volume were represented by changing COMPOUND visibility: the ability of OAT, PGP, and CYP to “see” and allow access to a

DMD Fast Forward. Published on October 20, 2008 as DOI: 10.1124/dmd.108.023820
This article has not been copyedited and formatted. The final version may differ from this version.

COMPOUND in its local neighborhood, which was specified by the value of *sitesN*. We did that by randomly shrinking the size of the local neighborhood (by one ELEMENT) from the initial value (ranging from 9 to 20 ELEMENTS) down to 2–4 ELEMENTS within the first ten MINUTES. The average decrement was one every two simulation cycles. The behavior of the version used to achieve SM-3 is graphed in Fig. 4B.

Having COMPOUND visibility decrease in combination with the above time-dependent changes in HEPATIC accessibility improved similarity, but was insufficient to achieve SM-2. Two further time-dependent changes were needed. We enabled PGP, CYP, and OAT to "die" (or to become inaccessible) randomly. We did that by assigning a probability, *defunctProb*, to each PGP, CYP, and OAT (but not a BINDER). It specified the probability that the object would become defunct during any given simulation cycle. When *defunctProb* = 0, each PGP, CYP, and OAT always functioned (as adjusted by *efficiencyProb*). We initially set *defunctProb* to a near-zero value and then increased it gradually thereafter following a quadratic relationship: $defunctProb(t) = initial\_defunctProb \bullet (defunctRate + t)/(defunctRate - t)$, where *initial_defunctProb* and *defunctRate* are two tunable parameters. The behavior of the version used to achieve SM-3 is graphed in Fig. 4C.

The decline in the ability of hepatocytes to metabolize digoxin or transport a compound (into or out of the cell), for whatever reason, was represented by decreasing the efficiency with which a CYP carried out its function. METABOLIC efficiency was specified by *efficiencyProb*; it controlled the probability that a CYP would function as intended. Its value was set initially to *efficiencyProb* = 0.95. We decreased *efficiencyProb* as the simulation progressed using an exponentially decreasing scaling factor to "slow" down the process. We added an additional condition: the minimum value of *efficiencyProb* was specified arbitrarily to be 0.03. The behavior of the version used to achieve SM-3 is graphed in Fig. 4D. The scaling method is detailed in Supplement.

These four time-variant mechanisms together helped us achieve SM-2, but not SM-3. Our best result using these four time-variant parameters is graphed in Supplement Fig. S8. In achieving SM-2, the

DMD Fast Forward. Published on October 20, 2008 as DOI: 10.1124/dmd.108.023820
This article has not been copyedited and formatted. The final version may differ from this version.

RISL was able to produce two important features: rapid decline of digoxin level in the perfusate, and rapid accumulation of metabolite early in the experiment.

Further Refinement of the Consequences of Liver Injury Achieved the Most Stringent Similarity Measure. After meeting SM-2, we strove to achieve SM-3. However, after exhaustive exploration of that RISL's parameter space, we failed to find a parameter vector that would move a METABOLITE profile closer to referent values without negatively affecting other profiles. For example, when we added more ENZYMES to S3 in an attempt to move the RIFAMPICIN PREDOSE METABOLITE time course up, the METABOLITE curves for DIGOXIN alone and for the QUINIDINE PREDOSE moved further up and outside the target range. Inspection of the original wet-lab data showed that, although the rate of digoxin uptake varied greatly due to uptake transporter inhibition by rifampicin, the amount of metabolite that formed early during perfusion was comparable. There was no measurement for metabolite at time = 0. In order to achieve SM-3 it was necessary to introduce further complexity to generate early levels of METABOLITE. As would be expected, doing so necessitated re-tuning most of the other parameter values.

What might have caused the early, high levels of metabolite in perfusate? We arrived at three alternative theories. 1) During pre-dose perfusion, prior to addition of digoxin, mild liver damage caused some cell lysates, including metabolic enzymes, to be released into perfusate. Even if metabolic activity released into perfusate was short-lived, it could have been sufficient to cause some digoxin metabolism. 2) Some digoxin metabolite may have already been present in the administered source material. 3) An endogenous factor (of hepatic origin) may have co-eluted with the metabolite during assay or cross-reacted with assay reagent. No evidence was available to rule out any of the three and detailed duplication of the same experiments was impracticable. Assertion of any one theory was expected to enable achieving SM-3. Because liver damage can release the contents of some hepatocytes into the perfusate, we elected to assert and explore that theory first. As we show below, doing so enabled achieving SM-3. Consequently, there was no reason to find parameterizations that would enable the other two theories to also achieve SM-3. To explore the plausibility of the first theory, we added different

DMD Fast Forward. Published on October 20, 2008 as DOI: 10.1124/dmd.108.023820
This article has not been copyedited and formatted. The final version may differ from this version.

numbers of differently parameterized ENZYMES to PERFUSATE prior to addition of DIGOXIN, and tested the consequences of a wide variety of parameterizations. The following specifications contributed to achieving SM-3. We added just four CYP to PERFUSATE, about 13% the total CYP in the S3. To reflect the different environment of these ENZYMES, we arbitrarily specified different ENZYME parameter values that were lower than CELLULAR ENZYMES: METABOLIC *efficiencyProb* = 0.3 (rather than 0.97) and *sitesN* = 12 (rather than 15). We specified a much higher *defunctProb* (0.025 rather than 0.0025). With that small addition and re-tuning of other parameters, we achieved SM-3. The results are presented in Fig. 3. The time-variant parameters are specified in Table 5; their values are graphed in Fig. 4.

Significance of Time-Variant Mechanisms. A crucial assumption when experimenting with in vitro systems, such as perfused livers, is that absent perturbing events that are part of the experimental design, hepatic functions will remain effectively constant over the duration of the experiment. By being forced to switch from time-invariant to time-variant mechanisms, we were representing a perfused liver whose behavior was inconsistent with that assumption. By turning off all injury-induced, time-variant mechanisms, and executing experiments, we observed plausible results for "normal" livers having constant function throughout the experiment. Those results are graphed in Fig. 5. In Supplement Figs. S10 and S11, we present eight examples of the consequences of turning off different aspects of the time-variant mechanisms. Together, these sets of RISL time-series data show how each time-variant mechanism contributes in distinctive ways to differences between Figs. 3 and 5.

Discovering the mechanisms used for Fig. 3 was an iterative and exploratory process that involved induction from both the referent data and—*importantly*—the structure and behavior of prior RISLs. The result is an example of a hybrid inductive–synthetic model that used a middle-out inductive strategy, appropriate for model usage.

Discussion

We first discuss characteristics of the RISL class of models relative to traditional PK models and then conclude with observations on the results. An objective of perfused liver experiments is to gain new

knowledge regarding details of hepatic disposition and metabolism. Hypotheses about those details are induced from the data. Fitting inductive mathematical models to the data is often used as evidence in support of particular hypotheses. To date, designing and conducting new wet-lab experiments has been the only practicable means to falsify experimentally those hypothesized mechanisms. The methods presented provide an additional experimental means of discovering and testing the plausibility of drug interaction details even when the mechanistic details change during the course of experiments.

A purpose in conducting experiments that provide time course data is often to shed light on prevailing mechanistic hypotheses about the dynamics. The methods described here provide a means to leverage the investment in those experiments by constructing and studying mechanistic analogues contemporaneously with wet-lab experiments. A traditional, inductive, PK model hypothesizes an explanation of patterns in PK data (Rescigno, 2001). The mathematics of physiologically based PK models describe data features predicted to arise from conceptualized mechanisms, which are typically described in sketches and prose. There is an unverifiable, conceptual mapping between equations and envisioned mechanisms, as illustrated on the left side of Fig. 1. The RISLs and the methods used are different. The synthetic modeling and simulation method (Hunt et al. 2006), (Fisher and Henzinger 2007), (Hunt et al. 2008), enables one to assemble software components into mechanisms as illustrated in Fig. 1. They provide an independent, scientific means to challenge, explore, and better understand any inductive mechanism and, importantly, the assumptions on which it rests.

Measures of RISL executions such as Fig. 3 provide a test of the mechanistic hypothesis instantiated in the RISL. An acceptable similarity between in silico and wet-lab data, mapping A in Fig. 1, is evidence that mapping B may exist between the dynamics occurring during simulation and corresponding dynamics thought to occur within perfused livers, even though the actual events and processes in the two systems are different. That mapping can be realistic, consistent with discretizations and the degree of abstraction. To the extent that mapping B is realistic, we can posit that the implemented mechanisms may have also had biological counterparts: mapping C.

DMD Fast Forward. Published on October 20, 2008 as DOI: 10.1124/dmd.108.023820
This article has not been copyedited and formatted. The final version may differ from this version.

RISL design features make it easy to reuse a mechanism in developing an explanation of other experimental details, past or future. As additional data or knowledge becomes available, the components comprising the mechanisms on the right side of Fig. 1 can be reused, much as we have done here, to explore alternative mechanisms and improve realism. Experimenting with RISLs enables the scientist to better understand the analogue mechanisms, with the expectation that that improved insight can translate to the referent system.

RISLs are designed to be relativistic for maximum flexibility. Their mechanisms are abstract analogues of their referents, not precise one-for-one renderings. For mapping A in Fig. 1 to be quantitative, as in Fig. 3, an additional model—a method of scaling—is needed to relate RISL observables directly to the wet-lab PK data. To make mappings B and C semiquantitative, an additional translational model is needed for each. By making the RISL relativistic, we can keep translational models separate from the RISL. If we were to move any one of these scaling models into the RISL, we would immediately reduce the RISL's flexibility, which is scientifically undesirable. The levels of temporal, spatial, and mechanistic granularity (which control resolution) are somewhat arbitrary: they need to be sufficiently fine so that the measured consequences of RISL execution meet a stringent SM. Granularity can be easily increased or decreased when that is needed. Because everything within the RISL is relativistic, an algorithm can be implemented when needed to automatically adjust parameter values to accommodate new levels of granularity so that the consequences of mechanisms can remain essentially the same.

The synthetic method of modeling and simulation is not intended for making quantitatively precise predictions about observables. Traditional, equation based PK models can already do that very well. The synthetic method is best suited for studying the observable consequences of interacting components and testing hypotheses about mechanisms. As demonstrated here, because any number of distinctly different compounds can be studied within the same experiment, RISLs and their methods are ideally suited for studying mechanisms of drug-drug interactions, and the results of this study have demonstrated their utility for doing that.

DMD Fast Forward. Published on October 20, 2008 as DOI: 10.1124/dmd.108.023820
This article has not been copyedited and formatted. The final version may differ from this version.

From a simulation perspective, it is demanding to expect one RISL mechanisms to simulate time course data for DIGOXIN and its METABOLITE that closely matches observed data from three different treatments. Because all of the mechanistic details are intertwined, a mechanistic change made to improve one profile automatically changes the others. Even though the RISL was relatively (to traditional PK models) fine-grained and hierarchical, having an RISL with only time-invariant mechanisms was too simple: it achieved SM-1, but not SM-2. Explorations of more complicated mechanisms lead to adding a METABOLITE TRANSPORTER to S2, including ENZYMES in PERFUSATE, and making the four time-variant changes in Fig. 4. 1) Accessibility (transitional state) of RIFAMPICIN, QUINIDINE, and DIGOXIN to HEPATIC surfaces (S2) decreased. 2) CYP became less efficient. 3) The probability that an OAT, PGP, or CYP would remain active in the next simulation cycle declined; and 4) the relative size of the neighborhood in which RIFAMPICIN, QUINIDINE, and DIGOXIN were visible to OAT, PGP, and CYP shrank. When implemented together within a RISL, we identified a parameterization that enabled successfully achieving SM-3 (Fig. 3). We submit that analogous changes in hepatic mechanisms occurred during the referent experiments: the livers were dying and/or increasing portions were being poorly perfused. Having the evidence presented influences how we think about and interpret the wet-lab results. Comparable insight cannot be achieved from purely inductive PK models. That is because components of traditional, physiological based PK model are concepts. As such, and as illustrated on the left side of Fig. 1, there can be no concrete mappings between model components, their parameterizations, and referent counterparts (Rescigno, 2001).

An important underlying assumption when conducting liver perfusion experiments is that liver function remains relatively constant over the course of experiments. An important observation is that it was necessary to posit time-variant mechanisms in order to account for the data in Fig. 3. Together, the specific time-variant mechanisms in Fig. 4, in the context of the RISL analogue in Fig. 2, comprise the one abstract explanation for the referent data that we discovered. Different variations on this same mechanistic theme may provide equally satisfactory explanations. If we were to use a different liver analogue, the In Silico Liver in (Yan et al., 2008a) for example, alternate, similarly plausible time-variant

mechanisms may be discovered. How mechanistic explanations may change between different models of the same system is an avenue for future research. In addition, there may be several, somewhat different parameter vectors for the implemented mechanisms that do equally well at achieving SM-3, but our search did not locate them. Taken together, the following five observations are circumstantial evidence that the mechanistic explanations offered are plausible. A single, time-variant RISL produced 1) simulated DIGOXIN and METABOLITE PERFUSATE levels that were quantitatively similar to referent data when digoxin was administered alone. 2) Simulated DIGOXIN and METABOLITE PERFUSATE levels following separate pretreatments with QUINIDINE and RIFAMPICIN achieved SM-3. 3) Measures of Monte Carlo variants of the RISL used for Fig. 3 had the same time course features observed in the wet-lab data. However, because of the built-in stochastic uncertainty, they lack the precision of traditional PK models. 4) Simulated QUINIDINE and RIFAMPICIN data were similar to referent time course data (see Supplement Fig. S5) 5) Modest changes in parameter vector values altered the relative positions of the six simulated perfusate profiles (not shown), but not their shapes. The RISL can therefore stand as a metaphor (an abstract analogue) of what may have occurred during the liver perfusion experiments.

Acknowledgements

We thank Prof. Leslie Z. Benet, Glen E.P. Ropella, Dr Yvonne, Y Lau, and members of the BioSystems and Benet groups for helpful discussion and commentary.

References

Bailey SM and Reinke LA (2000) Effect of low flow ischemia-reperfusion injury on liver function. *Life Sci* **66:** 1033-1044.

Booth CL, Brouwer KR, and Brouwer KL (1998) Effect of multidrug resistance modulators on the hepatobiliary disposition of doxorubicin in the isolated perfused rat liver. *Cancer Res* **58:** 3641-3648.

Booth CL, Pollack GM, and Brouwer KL (1996) Hepatobiliary disposition of valproic acid and valproate glucuronide: use of a pharmacokinetic model to examine the rate-limiting steps and potential sites of drug interactions. *Hepatology* **23:** 771-780.

Fisher J and Henzinger TA (2007) Executable cell biology. *Nat Biotechnol* **25:** 1239-1249.

Garmire LX, Garmire DG, and Hunt CA (2007) An in silico transwell device for the study of drug transport and drug-drug interactions. *Pharm Res* **24:** 2171-2186.

Hunt CA, Ropella GE, Yan L, Hung DY, and Roberts MS (2006) Physiologically based synthetic models1 of hepatic disposition. *J Pharmacokinet Pharmacodyn* **33:** 737-772.

Hunt CA, Ropella GEP, Park S, and Engelberg J (2008) The Real Dichotomies Between Computational and Math11ematical Models. *Nat Biotech* **26:** 737-738.

de Lannoy IA and Silverman M (1992) The MDR1 gene product, P-glycoprotein, mediates the transport of the cardiac glycoside, digoxin. *Biochem Biophys Res Commun* **189:** 551-557.

Lau YY, Wu CY, Okochi H, and Benet LZ (2004) Ex situ inhibition of hepatic uptake and efflux significantly changes metabolism: hepatic enzyme-transporter interplay. *J Pharmacol Exp Ther* **308:** 1040-1045.

Liu Y and Hunt CA (2006) Mechanistic study of the cellular interplay of transport and metabolism using the synthetic modeling method *Pharm Res* **23:** 493-505.

Matsuura Y, Nishi S, Kariya N, Shimadzu K, and Asada A (2001) The effects of norepinephrine and prostaglandin E1 on pharmacokinetics of lidocaine in isolated perfused rat liver. *Life Sci* **68:** 2123-2129.

Noé B, Hagenbuch B, Stieger B, and Meier PJ (1997) Isolation of a multispecific organic anion and cardiac glycoside transporter from rat brain. *Proc Natl Acad Sci USA* **94:** 10346-10350.

Rescigno A (2001) On the use of pharmacokinetic models. *Phys Med Biol* **49:** 4657–4676.

Sheikh-Bahae S and Hunt CA (2006) Prediction of in vitro hepatic biliary excretion using stochastic agent-based modeling and fuzzy clustering, in *Proceedings of the 37th Conference on Winter Simulation, Monterey, CA, Dec 03-06* (L. F. Perrone, et al., eds.) pp 1617-1624, INFORMS, Hanover, MD.

Straatsburg IH and Frederiks WM (1997) In situ analysis of ischaemia/reperfusion injury in rat liver studied in three different models. *Int J Exp Pathol* **78:** 149-161.

Tang J, Ley KF, and Hunt CA (2007) Dynamics of in silico leukocyte rolling, activation, and adhesion. *BMC Syst Biol* **1:** 14.

Tirona RG and Pang KS (1999) Bimolecular glutathione conjugation kinetics of ethacrynic acid in rat liver: in vitro and perfusion studies. *J Pharmacol Exp Ther* **290:** 1230-1241.

Yan L, Ropella GE, Park S, Roberts MS, and Hunt CA (2008a) Modeling and simulation of hepatic drug disposition using a physiologically based, multi-agent in silico liver. *Pharm Res* **25:** 1023-1036.

Yan L, Sheihk-Bahaei S, Park S, Ropella GE, and Hunt CA (2008b) Predictions of hepatic disposition properties using a mechanistically realistic, physiologically based model. *Drug Metab Dispos* **36:** 759-768.

Footnotes

This work was supported in part by grants provided by the CDH Research Foundation. The work was abstracted in part from a dissertation to be presented by TNL to the Graduate Division, University of California, San Francisco, CA, in partial fulfillment of the Ph.D. degree.

Legend for Figures

Figure 1. Relationships between wet-lab, perfused liver experiments, traditional PK models, and the RISLs. **Center**: rat livers in an experimental context are the referent systems. During experiments, lobular components interact with transiting drug molecules to cause changes in digoxin's concentration-time profile (and that of its primary metabolite). The system's behaviors during the experiment are reflected in the collected data. **Left**: the researcher identifies patterns in the wet-lab data. From those and prior PK knowledge, a mechanistic description of what is thought to have occurred during the experiment is induced, thus establishing an abstract, conceptual mappings from that description to hepatic mechanisms. The researcher offers a set of PK equations believed capable of describing the time course patterns identified in the data. A discretized, validated model of the equations in software is constructed and executed to simulate parameterized equation output. Metrics specify the goodness of fit of the simulated output to the data, and that establishes a concrete mapping from simulated output to wet-lab data. **Right**: The abstract mechanistic description (Fig. 2) is different from that on the left side. Software components are designed, coded, verified, and assembled and connected guided by that mechanistic description. The product of the process is a collection of mechanisms rendered in software. A clear mapping—C—is intended to exist between components and how they plug together, and hepatic physiological and microanatomical details. Relative similarity is controlled in part by parameterizations. Importantly, mapping C can be concretized iteratively. Compilation and source code execution gives rise to a working analogue. Its dynamics are intended to represent abstractly (mapping B) corresponding dynamics (believed to occur) within the liver during an experiment. Mapping B can also be concretized iteratively. Measures of simulated dynamics provide time series data that are intended to mimic corresponding measures of wet-lab perfusion experiments. Achieving SM-1, -2, and –3, enables mapping A to be made concrete.

DMD Fast Forward. Published on October 20, 2008 as DOI: 10.1124/dmd.108.023820
This article has not been copyedited and formatted. The final version may differ from this version.

Figure 2. Illustration of the Recirculating In Silico Liver (RISL) and its components. **A:** The RISL is represented as five concentric spaces (S1–S5) with S1 representing recirculating perfusate and rapidly equilibrating intrahepatic spaces. Each space is a 50x50 toroidal square grid. S2 represents barriers between S1 and S3. S3 maps to intracellular spaces. S4 represents barriers between S3 and S5. S5 maps to bile. ELEMENTS are containers for other objects. One is located at each grid location. Within a space, they have the same relative capacity, but capacity differs between spaces. The grid spaces shaded differently illustrate that each element can contain different objects. **B:** Shown are illustrations of four ELEMENTS, one each from S1-S4, with examples of the object they may contain. Different ELEMENT sizes illustrated different capacities. ELEMENTS can contain mobile and fixed objects. The spheres represent mobile COMPOUNDS; the different shadings illustrate the different states in which they can exist. A fixed OAT object is shown in the S2 element, and a fixed PGP object is shown in the S4 element. A stylized illustration of a multi-site CYP is shown in S3; one COMPOUND is shown bound. A stylized illustration of a multi-site binder is shown in S1.

Figure 3. Simulated results using RISLs with the time-variant mechanisms graphed in Fig. 4. Symbols are values reported in (Lau et al., 2004) of fraction of digoxin dose remaining in the perfusate for each of the three different sets of experiments (each set: $n = 6$); the bars are ± 1 SD for the wet-lab data. The curves are mean simulated values of 18 Monte Carlo executions of the RISL parameterized to exhibit time-variant mechanisms according to Tables 3–5. All parameterizations of a corresponding time-invariant RISL failed to achieve SM-3. The time-variant RISL differs in four ways from those simple, linear, time-invariant RISLs. 1) A METABOLITE-specific TRANSPORTER was added to S2 to increase the rate of return at early times of METABOLITE to PERFUSATE. 2) The accessibility of S2 to mobile DRUGS in PERFUSATE (S1 in Fig. 2) decreased with time as shown in Fig. 4A, and as specified in the text and in Supplement, decreasing the rate of both passive and active HEPATIC permeation by all three DRUGS. 3) The efficiency of CYP decreased with time as graphed in Fig. 4D. Such change can be caused by decreased viability or diminished perfusion or some combination. 4) In addition, a portion of CYP, OAT,

DMD Fast Forward. Published on October 20, 2008 as DOI: 10.1124/dmd.108.023820
This article has not been copyedited and formatted. The final version may differ from this version.

and PGP became inactive (Fig. 4C) each simulation cycle. A small number of less functional CYPs were added to S1 (perfusate) to mimic enzymes believed released from injured hepatocytes during system preparation. **A**: Shown is the mean (n = 18) DIGOXIN PERFUSATE levels for each of the three indicated treatments. In all three cases, simulated DIGOXIN values achieved SM-3; most were within a SD of referent values. **B**: Shown are the mean METABOLITE PERFUSATE levels corresponding to the three treatments in **A**. Again, most simulated values were within a SD of referent wet-lab data. Consequently, all simulated METABOLITE values achieved SM-3. Collectively, the six sets of simulated data in **A** and **B** also achieved SM-3.

Figure 4. Values of time-variant parameters. Each graph shows time-dependent parameter values used to generate the results shown in Fig. 3. **A**: The graph shows the time-variant values of the fraction of COMPOUNDS in S1 that were in the *transitional* state, which is defined in the text. **B**: Show are mean, time-dependent values of *sitesN* for CYP averaged over 10 CYP; the pattern of change was the same for PGP and OAT. Factors such as accessible hepatocyte surface area and effective cellular volume map to the ability of OAT, PGP, and CYP to "see," and allow access to, a COMPOUND in its local neighborhood. The initial values of *sitesN* for OAT, PGP, CYP, and MT were decremented randomly. The average decrement was one every two simulation cycles. The initial and minimum *sitesN* values were 22 and 2 for CYP, 9 and 4 for PGP, and 20 and 4 for OAT. **C**: Shows are time-dependent values of *defunctProb* for CYP. The pattern of change was the same for PGP and OAT, and was specified using the quadratic relationship specified in the text. Initial *defunctProb* values: 0.0042 (CYP), 0.00003 (PGP), and 0.0017 (OAT). In each case, the *defunctProb* value at 60 minutes was about three to four times that of the initial value. **D**: Shown are time-dependent values of METABOLIC *efficiencyProb*: initial = 0.95; minimum = 0.03. An algorithm described in Supplement was used to adjust the final value along with the early and subsequent exponential rate of decline. *EfficiencyProb* for PGP and OAT remained constant.

Figure 5. Simulation of results from an "ideal experimental liver." This RISL Shown are mean results (*n* = 12) for an RISL and experimental conditions that are the same as in Fig. 3, except that all time-variant parameter changes in Fig. 4 were turned off and no ENZYME was added to PERFUSATE.

DMD Fast Forward. Published on October 20, 2008 as DOI: 10.1124/dmd.108.023820
This article has not been copyedited and formatted. The final version may differ from this version.

Tables

Table 1. Comparing the perfused liver with the RISL, its in silico analogue

Biological Aspects; System Features	Analogue Components and Features
Form; space	GRIDS; ELEMENTS that function as containers
Function; mechanism	Sequence of events; data transforms in object methods and behaviors
Time	Simulation cycles
Drug (and inhibitor) molecules	Mobile objects: DRUGS, COMPOUNDS
Perfusate; experimental apparatus	SPACE S1; COMPOUNDS are in one of three states
Liver = many similar lobules	A number of simulations, averaged
Cell contents	ELEMENT objects assigned to SPACE S3
Bile	ELEMENT objects assigned to SPACE S5
Cell content–sinusoid interface	ELEMENT objects assigned to SPACE S2
Cell content–bile interface	ELEMENT objects assigned to SPACE S4
Metabolic enzymes and transporters	Stationary objects: CYP, OAT, PGP, MT, BINDERS
Mechanisms	Sequence of events
Passive dispersion	COMPOUNDS change location within SPACES
Passive transport	COMPOUNDS move between SPACES
Transport (active or facilitative)	COMPOUNDS moved by TRANSPORTERS
Metabolism	COMPOUNDS converted to METABOLITES
Binding	COMPOUNDS attaching to BINDERS
Measures taken during experiments	Measures taken during experiments
Hypothesis; hypothesis testing	A specific analogue; a set of simulations

Table 2. Primary parameters of the Recirculating In Silico Liver (RISL) system

System Parameters	Remarks	Values
systemSize	Size of SPACES S1–S5	50 x 50
numSolute	Dose: number of SUBSTRATES: DIGOXINS	1,000
numInhibitor	Dose: number of INHIBITORS: RIFAMPCIINS or QUINIDINES	2,000
adminTimeSolute	Administration time of SUBSTRATE	60
adminTimeInhibitor	Administration time of INIHIBITOR	0
insilicoPH	In silico pH of SPACES	7.4
numPgps	Number of PGP	30
numOats	Number of OAT	100
numCyps	Number of CYP (ENZYMES)	30
numBinders	Number of BINDERS	75
numMTransporters	Number of METABOLITE TRANSPORTER (MT)	100
timestepfactor [a]	Scaling factor for passive permeation	2.0
internalProb	Flow rate: probability of a compound in S1 being *internal* to the liver; simulates flow from bulk perfusate into sinusoidal spaces	0.13
maxSites	Number of substrate binding sites per stationary object	2-10
efficiencyProb [b]	Efficiency parameter for CYP, PGP, and OAT	
sitesN [b]	Size of neighborhood: number of adjacent ELEMENTS scanned each cycle by CYP, PGP, and OAT	
defunctProb [b]	Probability of going *defunct* within the simulation cycle	

[a] See Supplemental Material for a detailed explanation.

[b] Denotes time-variant parameters: see Table 5

DMD Fast Forward. Published on October 20, 2008 as DOI: 10.1124/dmd.108.023820
This article has not been copyedited and formatted. The final version may differ from this version.

Table 3. Compound specific parameters values

COMPOUND Parameters	Remarks		Values DIGOXIN [a]	RIFAMPICIN [a]	QUINIDINE [a]	METABOLITE [b]
MW [c]	molecular weight of the solute		781	822	324	601
logP [c]	logP - common logarithm of octanol/water partition coefficient		1.14	3.60	2.53	1.60
pKa [c]	pKa closest to *insilicoPH*		13.5	6.9	8.6	13.5
inihibitorType	uptake inihibitor? True/False		n/a	TRUE	FALSE	n/a
closeToInterface	Fraction sufficiently close to interface such that it is *transitional* [d]	S1	--[e]	0.75	0.75	0.10
		S3	0.10	0.02	0.04	0.10
		S5	0.10	0.05	0.05	0.10
transitProb	Initial estimates of trans-membrane transit probabilities, after scaling by *timestepfactor*	S1→S2	0.066	0.069	0.102	0.078
		S2→S1	0.123	0.007	0.099	0.068
		S2→S3	0.123	0.007	0.088	0.068
		S3→S2	0.066	0.069	0.104	0.078
		S3→S4	0.066	0.069	0.104	0.078
		S4→S3	0.123	0.007	0.090	0.068
		S4→S5	0.123	0.008	0.060	0.068
		S5→S4	0.066	0.069	0.106	0.078

[a] Physicochemical properties reflect those of the referent drug.

[b] Physicochemical properties reflect those of digoxigenin bis-digitoxoside.

[c] Molecular weight, logP, and pKa are used in calculating the initial, passive transit probabilities, as described in Supplemental Material. For pKa, only the value closest to 7.4 is listed.

[d] The *closeToInterface* value for all solutes in S2 and S4 was always 1. This reflects the fact that the referent barriers are sufficiently thin so that *all* solutes within them at the start of a 10 second interval (a simulation cycle) will have had an opportunity to transition by the end of that interval. For all spaces except S1, *closeToInferace* is the *fraction transitional*

[e] *CloseToInterface* for S1 is a time-variant parameter. It, together with *internalProb*, specifies the *fraction transitional* (Table 5).

DMD Fast Forward. Published on October 20, 2008 as DOI: 10.1124/dmd.108.023820
This article has not been copyedited and formatted. The final version may differ from this version.

Table 4. Parameters for COMPOUND-PROTEIN interactions

COMPOUND-PROTEIN Interaction		**Values**			
Parameters		**DIGOXIN**	**RIFAMPICIN**	**QUINIDINE**	**METABOLITE**
	MT	FALSE	FALSE	FALSE	TRUE
isaSubstrate	PGP	TRUE	FALSE	FALSE	TRUE
substrate of ?	OAT	TRUE	TRUE	FALSE	TRUE
TRUE / FALSE	CYP	TRUE	FALSE	FALSE	FALSE
	BINDER	FALSE	FALSE	FALSE	FALSE
	MT	0	0	0	0.9
assocProb	PGP	0.4	0	0.9	0.4
reflects binding	OAT	0.75	0.7	0	0.05
affinity to protein	CYP	0.5	0	0	0
	BINDER	0.3	0	0	0.5
	MT	1.0[a]	1.0[a]	1.0[a]	0.9
releaseProb	PGP	0.7	1.0[a]	0.04	0.7
reflects dissociation	OAT	0.8	0.05	1.0[a]	0.9
from protein	CYP	0.2	1.0[a]	1.0[a]	1.0
	BINDER	0.1	1.0[a]	1.0[a]	0.01

[a] Not used because *assocProb* = 0.

DMD Fast Forward. Published on October 20, 2008 as DOI: 10.1124/dmd.108.023820
This article has not been copyedited and formatted. The final version may differ from this version.

Table 5. Time-variant parameters

Time-variant parameter			Initial value	Terminal value
Effective SURFACE AREA changes	*Fraction transitional* [a] in S1		0.13	0.052
	sitesN (neighborhood)	CYP	22	2
		PGP	9	4
		OAT	20	4
		MT	25	4
METABOLIC and TRANSPORT activity changes	*efficiencyProb* [a]	CYP	0.95	0.03
		PGP	1	1
		OAT	0.65	0.65
		MT	1	1
	defunctProb	CYP	0.0042	0.018
		PGP	0.0003	0.001
		OAT	0.0017	0.0057
		MT	0.0003	0.001

[a] The method for changing *fraction transitional* and *efficiencyProb* (Fig. 4A and 4D) is detailed in Supplemental, under Parameter scaling.

Figure 1

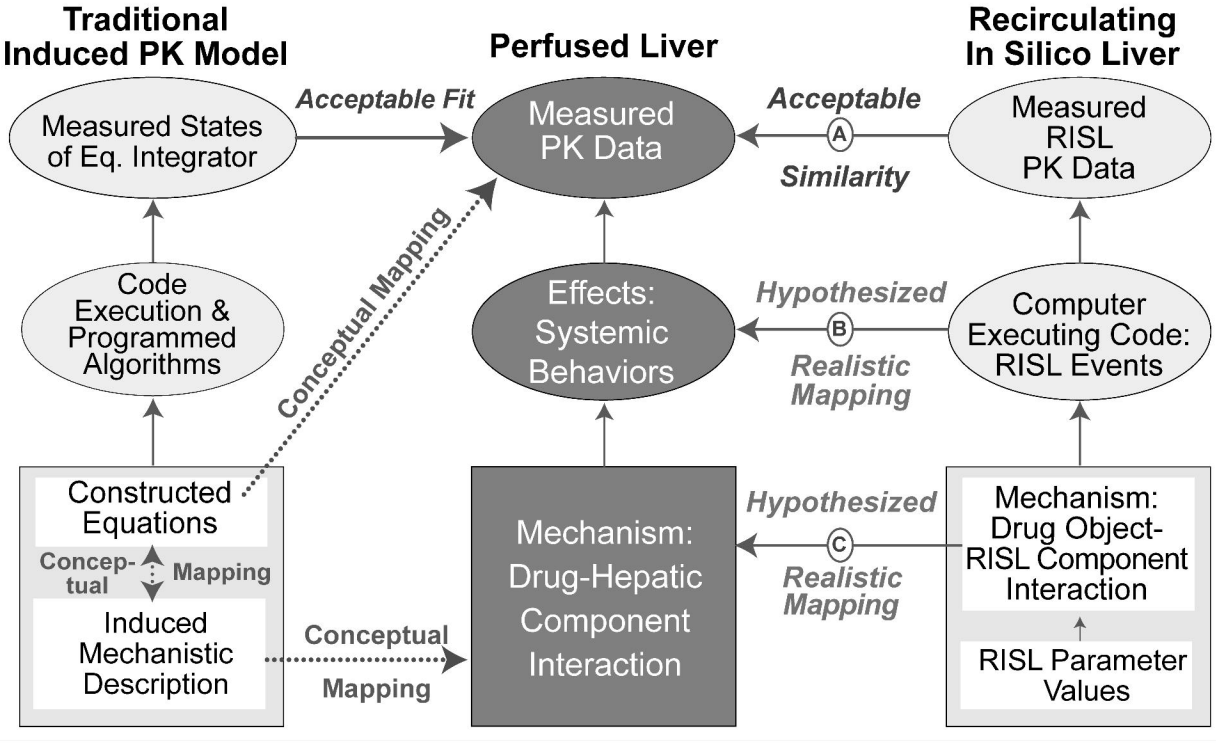

Figure 2

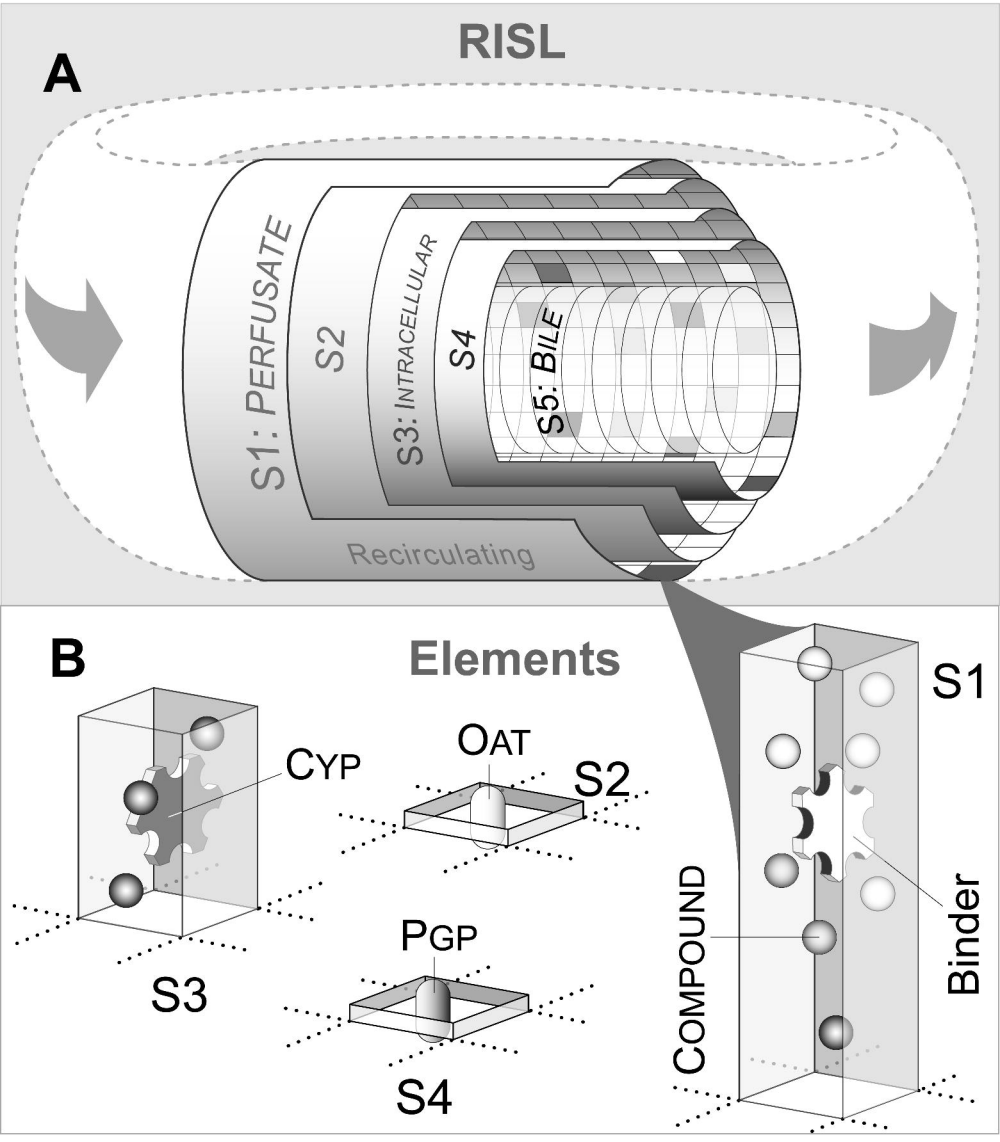

Figure 3

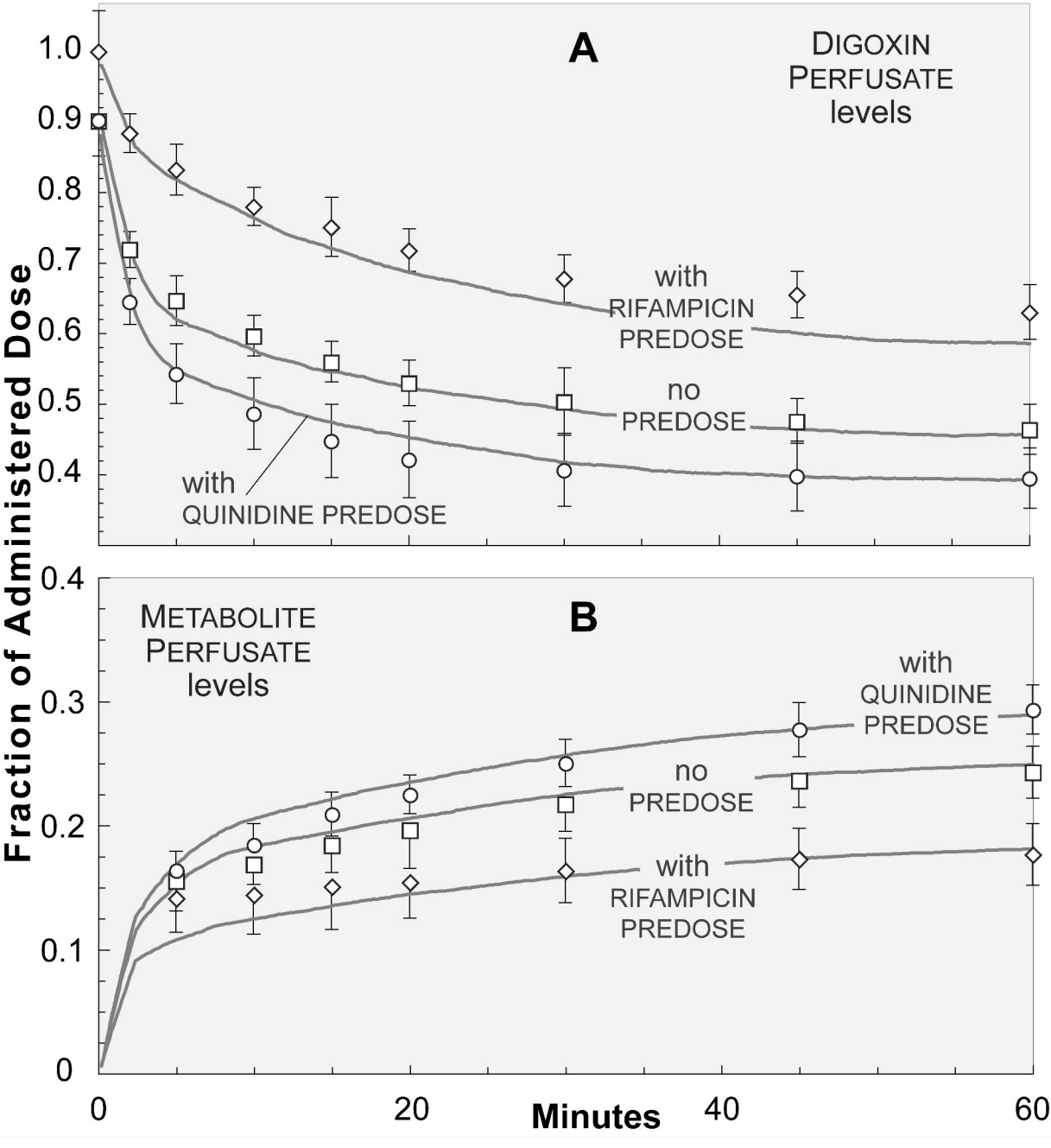

Figure 4

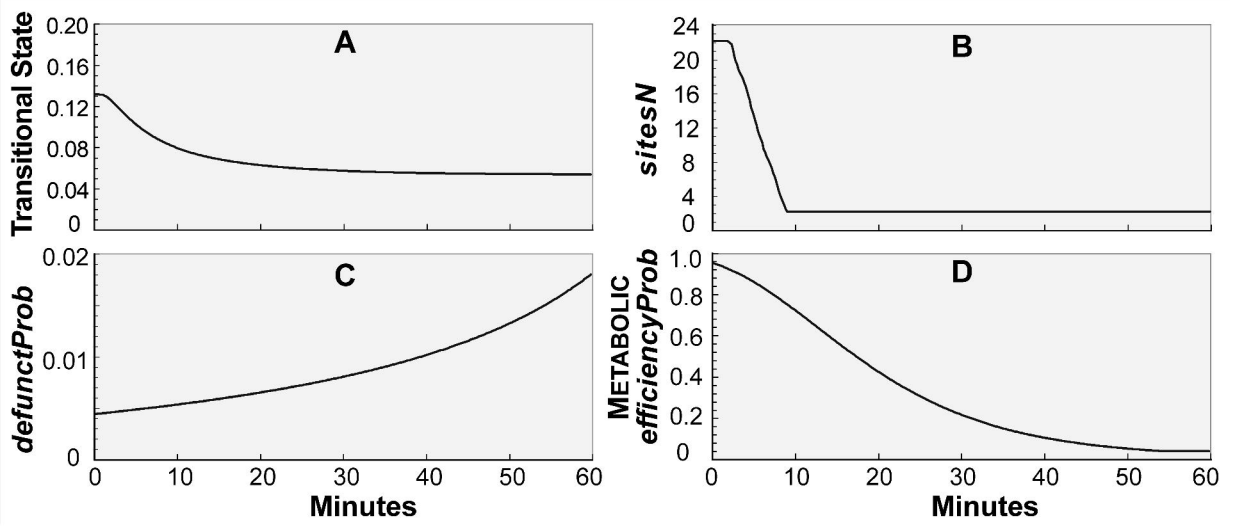

Figure 3